6430–6442 *Nucleic Acids Research, 2023, Vol. 51, No. 12* *Published online 11 May 2023*
https://doi.org/10.1093/nar/gkad362

Conformational dynamics of the RNA binding channel regulates loading and translocation of the DEAH-box helicase Prp43

Marieke Enders, Ralf Ficner and Sarah Adio*

Department of Molecular Structural Biology, Institute of Microbiology and Genetics, Georg- August-University Göttingen, Justus-von-Liebig-Weg 11, D-37077 Göttingen, Germany

Received November 25, 2022; Revised April 08, 2023; Editorial Decision April 20, 2023; Accepted April 30, 2023

ABSTRACT

The DEAH-box helicase Prp43 has essential functions in pre-mRNA splicing and ribosome biogenesis, remodeling structured RNAs. To initiate unwinding, Prp43 must first accommodate a single-stranded RNA segment into its RNA binding channel. This allows translocation of the helicase on the RNA. G-patch (gp) factors activate Prp43 in its cellular context enhancing the intrinsically low ATPase and RNA unwinding activity. It is unclear how the RNA loading process is accomplished by Prp43 and how it is regulated by its substrates, ATP and RNA, and the G-patch partners. We developed single-molecule (sm) FRET reporters on Prp43 from *Chaetomium thermophilum* to monitor the conformational dynamics of the RNA binding channel in Prp43 in real-time. We show that the channel can alternate between open and closed conformations. Binding of Pfa1(gp) and ATP shifts the distribution of states towards channel opening, facilitating the accommodation of RNA. After completion of the loading process, the channel remains firmly closed during successive cycles of ATP hydrolysis, ensuring stable interaction with the RNA and processive translocation. Without Pfa1(gp), it remains predominantly closed preventing efficient RNA loading. Our data reveal how the ligands of Prp43 regulate the structural dynamics of the RNA binding channel controlling the initial binding of RNA.

GRAPHICAL ABSTRACT

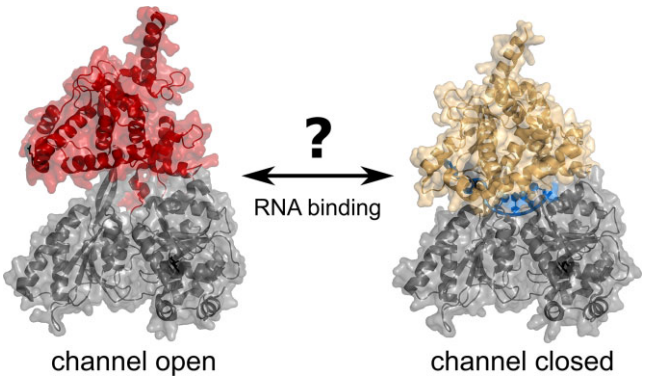

INTRODUCTION

The DEAH-box helicase Prp43 remodels structured RNAs and RNA-protein complexes (RNPs) on ribosome precursor complexes and the spliceosome (1). Members of the DEAH-box helicase family reorganize their substrates through ATP-dependent motility in 3′ to 5′ direction along single-strands (2,3). During maturation of 60S ribosome subunits, Prp43 releases small nucleolar RNAs from their pre-mRNA binding sites (4–6), and it promotes the processing of 20S to 18S rRNA in precursors of the 40S ribosome (7,8). During the late states of splicing, Prp43 disassembles the intron lariat complex and disrupts stalled spliceosomes bound to pre-messenger RNA (mRNA) with suboptimal or erroneous splice sites, thus playing a key role in mRNA quality control (9–14). In the absence of binding partners provided by ribosome or spliceosome complexes, the affinity of Prp43 for RNA is low, and the ability to unwind structured RNA is negligible (10,15–18). G-patch (gp) proteins recruit the helicase to its cellular target sites, where they locally stimulate helicase and ATPase activity (4–9,16,19,20). Interestingly, the conserved glycine-rich consensus sequence motif shared by all the G-patch proteins is sufficient to achieve efficient stimulation (4,5,8,16,19,21). We have recently demonstrated that the G-patch motif of

*To whom correspondence should be addressed. Tel: +49 15734939778; Email: sarah.adio@uni-goettingen.de

Pfa1 (Pfa1(gp)) enables Prp43 to translocate processively along the RNA, controlling the movement of its RecA domains such that dissociation from the substrate is prevented during turnover (18).

Still, it remains unresolved how Prp43 gains access to its specific RNA substrates which often lie buried in the interior of complex RNA structures or RNPs. Efficient unwinding of double stranded RNA (dsRNA) by DEAH-box helicases requires a loading step onto a single stranded RNA (ssRNA) overhang preceding the duplex (22–24). The ssRNA is accommodated in a binding channel located between the two RecA domains comprising the helicase core and the C-terminal domains, mostly by contacts with the sugar-phosphate backbone, resulting in sequence-independent interaction (15–17). How the ssRNA strands enter the channel when Prp43 is part of cellular complexes is poorly understood. It can either insert through the narrow opening formed by the RecA2 and the C-terminal helix bundle (HB) and oligosaccharide binding (OB) domains, which is unlikely, or the entire channel widens up into a groove that can then fold around the RNA. Support for the latter idea comes from crystal structures of Prp43 bound to the ATP analog $ADPBeF_3^-$, which show the RNA binding channel in an open conformation (16). In these structures, the center of mass of the C-terminal HB and OB domains is shifted by approximately 15 Å with respect to the helicase core while the winged helix (WH) domain acts as a hinge between the RecA2 and the HB domain. The opening of the RNA binding channel is essential for Prp43 function as mutations trapping the channel in the closed conformation severely limit the unwinding activity (16). Together, these findings suggest a nucleotide-dependent RNA loading mechanism where ATP binding induces the opening of the channel such that ssRNA can enter in a single step. The subsequent closure of the channel around the RNA as seen in the Prp43—$ADPBeFe_3^-$—RNA complex would prime the helicase for translocation along the substrate (16). Although this mechanism seems plausible on first sight, it is not fully consistent with structural studies on other DEAH-box helicases. So far, the only other DEAH-box helicase observed with an open RNA binding channel is Dhr1 (DHX37 in humans) in the absence of ligands and co-factors (25). Nucleotide-dependent RNA loading is only compatible with this structure assuming a dynamic equilibrium of open and closed states, which is shifted in favor of the open state by the binding of ATP. The channel is closed in structures of DHX15, (the human homolog of Prp43) in complex with NKRF(gp) with and without ADP (26). The G-patch connects the RecA2 and WH domains of the helicase across the back side of the RNA binding channel and induces no apparent changes in this region, suggesting it does not promote the opening of the channel. On the other hand, G-patch binding substantially strengthens the affinity of Prp43 for RNA from the μM to the nM range, which indicates that it has a massive impact on the RNA binding properties of the enzyme (18,26,27). Whether this also effects the initial RNA binding step was not addressed so far and structures of helicase-G-patch-complexes with an open channel are not available. We have shown previously that when Prp43 undergoes successive cycles of ATP hydrolysis to processively translocate on the RNA, the likelihood for dissociation is highest in the ADP-state while it is much lower in the nucleotide-free and ATP-bound states (18). Tight RNA binding of Prp43—ATP disagrees with ATP induced channel opening unless further contacts govern the movement of the channel. Evidence proving the relevance of channel opening for RNA loading is lacking not only for members of the DEAH-box family but also for other subclasses of RNA helicases. This is mainly due to the absence of information on the structural dynamics of their RNA binding channel during interaction with their binding partners, including the natural ATP substrate. The understanding how their activation is primarily achieved and how regulation of helicases with similar architecture of the RNA binding, for example the viral NS3 helicases, is accomplished is therefore limited (28).

Here, we use single molecule Förster Resonance Energy Transfer (smFRET) to monitor the conformational dynamics of the RNA binding channel of Prp43 from *Chaetomium* thermophilum in real-time using total internal reflection of fluorescence (TIRF) microscopy. Our results demonstrate the relevance of the channel conformation for the initial RNA loading step. We show that in the absence of binding partners the channel can alternate between open and closed states. While the channel is mainly closed in the apo state, binding of ATP and Pfa1(gp), the cellular activators of the helicase, shifts the equilibrium towards the open state, allowing the accommodation of ssRNA. When the loading step is accomplished, the channel remains exclusively in the closed state, as required for processive translocation, until Prp43 reaches the end of the RNA strand. In the absence of Pfa1(gp), efficient loading does not take place. Our data explain the role of channel opening for Prp43 function and allow the integration of different channel conformations into a mechanistic model of the RNA loading process by DEAH-box helicases.

MATERIALS AND METHODS

Protein expression and purification

The homologues of Prp43 and Pfa1 from C. thermophilum (ctPrp43, ctPfa1) are annotated as 'hypothetical protein CTHT_0005780' and 'hypothetical protein CTHT_0048220'. Full-length ctPrp43 and the gp motif of ctPfa1 (residues 662–742) were cloned from genomic DNA of *C. thermophilum* var. *thermophilum* DSM 1495 into pGEX-6P-1 (29). For ctPrp43, a C-terminal non-cleavable His_6-tag was added to the GST-fusion protein by site-directed mutagenesis. ctPrp43 and ctPfa(gp) constructs were recombinantly expressed in Rosetta 2 (DE3) cells using an autoinduction protocol adapted from Studier (30) and purified by affinity chromatography followed by size exclusion chromatography as described in (18).

Fluorescence-labeling of ctPrp43

To generate two maleimide-reactive fluorescence-labeling sites in ctPrp43, eight native cysteine residues had to be considered. C148, C214, and C377 are buried inside the protein and inaccessible to the coupling group. C303, C323, C441, C508 and C543 are surface exposed and therefore accessible to the fluorescence dye. They were replaced by

site directed mutagenesis (C303T, C323V, C441A, C508A and C543S). The labeling sites were generated by introducing cysteine residues at position K170 in the RecA1 and E602 in the WH. The mutant protein was expressed and purified as described in (18). The purified protein was mixed with Cy3-maleimeide and Cy5-maleimide (Cytiva), dissolved in dimethylsulfoxide at a molar ratio of 1:2:2 (protein:Cy3:Cy5) and incubated for 30 min at 20°C. Excess dye was removed by Ni-sepharose affinity chromatography, labeled protein was eluted in 50 mM Tris/HCl (pH 7.5), 400 mM NaCl, 5% (v/v) glycerol, 2 mM $MgCl_2$, 250 mM imidazole. The labeled protein was dialyzed twice against 50 mM Tris–HCl, pH 7.5, 300 mM KCl, 3 mM $MgCl_2$ using Slide-A Lyzer Dialysis Cassette G2 3.5K (Thermo) for 1 h at 4°C. The labeled protein was concentrated to final concentrations between 40 and 70 μM (Amicon Ultra 50K, Millipore).

Determination of dye to protein ratio

To determine the degree of labeling, i.e. the average number of fluorophore molecules per molecule Prp43, the absorption of the labeled protein was measured at 280 nm as well as at the absorption maxima of Cy3 and Cy5, 552 nm and 650 nm. Both Cy3 and Cy5 also show absorption at 280 nm, thereby increasing the A_{280} for the labeled protein. The correction factors (CF) required to eliminate the contribution of the dyes at 280 nm were provided by the manufacturer as $CF_{Cy3} = 0.08$ and $CF_{Cy5} = 0.05$ (Cytiva). The dye to protein ratio was then calculated for both dyes using

$$c\ (Prp43) = \frac{A_{280} - \left[CF_{Cy3} \cdot A_{552}\right] - \left[CF_{Cy5} \cdot A_{650}\right]}{\varepsilon_{280}},$$

$$\frac{D}{P}\ (Cy3) = \frac{\frac{A_{552}}{\varepsilon_{552}}}{c(Prp43)} \wedge \frac{D}{P} \quad (Cy5) = \frac{\frac{A_{650}}{\varepsilon_{650}}}{c\,(Prp43)}$$

where A_{xxx} is the absorption of labeled Prp43 at the specified wavelength, ϵ_{280} is the extinction coefficient of Prp43 at 280 nm, and $\epsilon_{552} = 150\,000\ M^{-1}\ cm^{-1}$ and $\epsilon_{650} = 250\,000\ M^{-1}\ cm^{-1}$ are the extinction coefficients of Cy3 and Cy5 at their absorption maxima. $Prp43_{Cys}$ was labeled to 81% with Cy3 and to 98% with Cy5.

Sample preparation for TIRF microscopy

Cover slips and objective slides were cleaned by bath sonication in 1 M KOH and exposure to plasma (FEMTO plasma cleaner, Diener Electronic GmbH, Germany). Surfaces were then silanized by sonication in 3.9 mM N1-[3-(trimethoxysilyl) propyl] diethylenetriamine (Sigma-Aldrich) and 1.7 mM acetic acid, and baked for 20 min at 110 °C. PEG/PEG-Biotin functionalization of silanized surfaces was carried out by incubation with 20 mM PEG-NHS (MeO-PEG-NHS, IRIS Biotech GmbH, PEG1165), 0.2 mM Biotin-PEG-NHS (IRIS Biotech, PEG1057) and 20 mM KOH in 100 mM H_3BO_3 solution for 1 h at room temperature. Excess PEG was removed by washing with H_2O. Cover slips were dried at 60°C and stored under vacuum. For TIRF experiments, flow chambers were generated by combining objective slides and cover slips with double-sided sticky tape.

The Prp43-Pfa1(gp) complex was formed by incubating 1 μM labeled Prp43 with 5 μM Pfa1(gp) in TIRF buffer A (50 mM Tris–HCl, pH 7.5, 300 mM KCl, 3 mM $MgCl_2$) for 10 min at room temperature. Prior to the experiment, the complex was diluted to 1 nM Prp43 with TIRF buffer supplemented with 5 μM Pfa1(gp). For experiments without Pfa1(gp), labeled Prp43 was diluted to 1 nM with TIRF buffer A. Biotin/PEG-functionalized cover slips were incubated for 5 min at room temperature with TIRF buffer A containing additionally 10 mg ml^{-1} BSA and 1 μM neutravidin (Thermo Fischer Scientific). Excess neutravidin was removed by washing the cover slip with the same buffer containing 1 mg ml^{-1} BSA. A biotinylated anti-His antibody (Rabbit monochlonal, Sigma) was applied at 1.25 μg/ml to the cover slip. Excess antibody was removed by washing with TIRF buffer A containing 1 mg ml^{-1} BSA. Labeled Prp43 or Prp43-Pfa1(gp) complex was applied to the surface and incubated for 1 min at room temperature. Images were recorded after washing with TIRF buffer C (TIRF buffer A with 2.5 mM protocatechuic acid, 0.1 U/ml protocatechuate-3,4-dioxygenase (from Pseudomonas), 1 mM trolox (6-hydroxy-2,5,7,8-tetramethylchromane-2-carboxylic acid) and 1 mM methylviologen). To study the influence of ssRNA, ADP, AMPPNP or ATP, the imaging buffer was supplemented with 50 μg/ml PolyU RNA (Sigma Aldrich), 5μM U_{12} RNA (Axolabs), 2 mM ADP, 2 mM AMPPNP or 2 mM ATP. RNA fragments shorter than 12 nucleotides (U_X) were generated by sonication with a 250 sonifier for 30 min (Branson). To ensure a constant concentration of ATP during turnover, the imaging buffer was additionally supplemented with 10 U/ml pyruvate kinase and 3 mM phosphoenolpyruvate.

TIRF microscopy

TIRF imaging was performed on an IX 81 inverted microscope using a PLAPON 60× 1.45 numerical aperture objective (Olympus). Fluorescence was excited by a 561 nm solid-state laser operated at a power of 25 mW. Images were recorded with an electron multiplying CCD (charge-coupled device) camera (CCD-C9100-13, Hamamatsu). In FRET experiments, color channels were separated by projecting donor and acceptor emission on different parts of the CCD chip using an image splitter (dual view micro imager DV2, Photometrics), filter specifications HQ 605/40, HQ 680/30 (Chroma Technology). Movies were recorded at a rate of 30 frames per second. The experiments were carried out at 22°C.

Data analysis

Fluorescence time courses for donor (Cy3) and acceptor (Cy5) were extracted using custom-made Matlab (MathWorks) software as described (31,32). A semi-automated algorithm (Matlab) was used to select anti-correlated fluorescence traces (correlation coefficient < 0.1) exhibiting characteristic single fluorophore intensities. The bleed-through of Cy3 signal into the Cy5 channel was corrected using an

experimentally determined coefficient (~0.13 in our setup; (31)). All trajectories were smoothed over three data points and truncated to remove photobleaching and photoblinking events. Traces with lifetimes of Cy3 or Cy5 less than 20 frames (0.66 s) or with multiple photobleaching steps were excluded from the analysis. The FRET efficiency (E_{FRET}) was defined as the ratio of the measured emission intensities, Cy5/(Cy3 + Cy5) (32). FRET time courses were fitted by Hidden Markov modeling using the vbFRET software package (http://vbfret.sourceforge.net/) (33). Models with different number of states were considered for each data set. FRET changes of <0.1 in idealized trajectories were not considered as transitions. Transitions lasting for only one frame were not included in the analysis as well. About 5% of all traces were poorly idealized by Hidden Markov modelling and eliminated from subsequent analysis. Two-dimensional contour plots were generated from time-resolved FRET trajectories. The set of all FRET traces for a given condition was compiled in a histogram, which was fitted to a sum of Gaussian functions using Matlab code (31). Mean FRET values (mean ± sd) and population distribution (p = area under the curve ± sd) were calculated from three independent datasets and are summarized in Supplementary Table S1.

ATPase activity assay

ATP turnover by Prp43 was monitored using a coupled enzymatic assay following nicotinamide adenine dinucleotide (NADH) absorption at 340 nm over time in a VICTOR Nivo Multimode Microplate Reader (PerkinElmer) (34). Triplicate measurements were performed at room temperature in 20 mM Tris/HCl (pH 7.5), 150 mM KCl and 3 mM $MgCl_2$,250 nM NADH, 500 nM phosphoenolpyruvate, 6–8.3 U/ml pyruvate kinase and 9–14 U/ml lactic dehydrogenase at saturating ATP concentration of 2 mM. To obtain suitable reaction velocities, Prp43 was used at a concentration of 2 μM (no stimulation), 0.5 μM (stimulation with Pfa1(gp)) or 0.2 μM (stimulation with Pfa1(gp) and RNA). For measurements in the presence of Pfa1(gp) a 5-fold molar excess over Prp43 was used. Measurements in the presence of RNA were conducted at a concentration of 50 μg/ml PolyU RNA (Sigma). The ATP consumption per minute (k_{obs}) was calculated using

$$k_{obs} = \frac{\left[\frac{\Delta A_{340}}{\Delta t}\right]}{\varepsilon_{340} \cdot d \cdot c}$$

where $\Delta A_{340}/\Delta t$ is the slope of the NADH decrease, ϵ_{340} is the extinction coefficient of NADH, d is the optical pathlength and c is the protein concentration.

RNA binding assay

The RNA binding of Prp43 was measured by fluorescence polarization spectroscopy using a VICTOR Nivo Multimode Microplate Reader (PerkinElmer). The binding of 6 nM 3′ 6-carboxyfluorescein-labeled U_{12}-RNA to up to 200 μM Prp43 was monitored in triplicates at room temperature in 20 mM Tris/HCl (pH 7.5), 200 mM NaCl, 5% glycerol and 3 mM $MgCl_2$. For measurements in presence of Pfa(gp), the complex was formed by adding a 5-fold molar excess over Prp43 and incubating for 15 min at room temperature. The excitation wavelength was 480 nm and the emission was detected at 530 nm for 500 ms. The data were normalized by setting the maximum of measured polarization to 100% and the polarization measured without the addition of protein to 0%. The data were fitted by nonlinear regression with a sigmoidal dose response equation

$$r = r_0 + \frac{\Delta r_{max}}{1 + \left(\frac{[E]_T}{K_D}\right)^p}$$

where r is the measured polarization, r_0 the initial polarization, Δr_{max} the maximum amplitude of polarization, $[E]_T$ the total protein concentration and K_D the dissociation constant, using the analysis software OriginPro 9.1.

RNA unwinding assay

A fluorescence-based unwinding assay was used to monitor the RNA unwinding activity of Prp43. The substrates contained a 14 bp duplex flanked by various single-stranded overhangs (Eurofins genomics). One strand was labeled with Atto 488 at the 5′-end, while an Eclipse Quencher was attached to the 3′-end of the complementary strand.

- D0: 5′-(Atto488)CUACGUGGUCGUAG
- D3: 5′-(Atto488)CUACGUGGUCGUAGCAA
- D8: 5′-(Atto488)CUACGUGGUCGUAGCAACAACA
- D15: 5′-(Atto488)CUACGUGGUCGUAGCAACAA CAACAACAA
- Q[uni]: 5′-CUACGACCACGUAG(Eclipse)
- Q-8: 5′-CAACAACACUACGACCACGUAG(Eclipse)

For annealing, the strands were mixed at a ratio of 1:1.2 (dye:quencher), incubated for 5 min at 95°C and subsequently cooled to room temperature. *Q*[uni] was annealed with D0, D3, D8 or D15 to produce constructs with a 3′-overhang or blunt ends, while Q-8 was annealed with D0 to form a construct with a 5′-overhang. To monitor unwinding, 100 nM of RNA substrate was preincubated for 10 min at room temperature with 50 nM Prp43 in 20 mM Tris/HCl (pH 7.5), 150 mM KCl and 3 mM $MgCl_2$, in presence or absence of a 5-fold molar excess of Pfa1(gp). The reaction was stated by mixing with ATP to a final concentration of 1 mM. The fluorescence of the Atto 488 dye was excited at 470 nm and the emission was detected at 520 nm, using a Fluoromax III Spectrofluorometer (Horiba Jobin Yvon). The reaction was followed for 120 s. Strand separation is reported by dequenching of the ATTO488 fluorophore. The separated single strands form internal stem loops to prevent reannealing. The helicase reaction speed (k_{obs}) was calculated using the initial slope (0–15s) of each reaction as described in (35).

RESULTS

RNA duplex separation by the Prp43-Pfa1(gp) complex

Previous studies suggested that Prp43 requires stable binding of single stranded RNA at the 3′ end of duplex structures to separate them efficiently and showed that RNA

unwinding by the closely related helicase Prp22 is abolished in the absence of a single stranded 3′ overhang (16–18,22). We tested the unwinding of RNA substrates with different lengths and position of the single-strand structure in order to define the parameters of duplex unwinding for Prp43 (Figure 1). All substrates contain a 14 base pair duplex region where the top strand is labeled with the Atto 488 fluorophore at the 5′-end the bottom strand is labeled with the Eclipse Quencher at the 3′-end (Figure 1A). Separation of RNA strands was monitored by the increase (dequenching) of Atto488 fluorescence upon addition of ATP and the Prp43-Pfa1(gp) complex. The helicase unwinds the duplex with a 15 nt single-stranded 3′-overhang fast and efficiently (k_{obs} = 4.6 min^{-1}, Figure 1B) and the duplex with the 8 nt overhang with reduced rate (k_{obs} = 1.2 min^{-1}, Figure 1B). No unwinding was observed for the substrates containing a 3 nt 3′-overhang, a 15 nt overhang at the 5′ end, or blunt ends (Figure 1B). Together, these results show that Prp43 requires binding of a single stranded 3′-overhang to unwind duplex RNA with 3′-5′ polarity. Single-stranded regions that are significantly shorter than the footprint of Prp43 (i.e. the 3 nt (3′) construct) do not facilitate unwinding, indicating that the helicase requires binding of more nucleotides to initiate strand separation. Substrates with longer 3′-overhangs (i.e. the 15 nt (3′) construct) allow binding of more than one Prp43 molecule and presumably counteract reannealing which is why unwinding appears to occur with slightly increased rate.

smFRET label positions on Prp43 to monitor the structural dynamics of the RNA binding channel

To monitor the structural dynamics of the RNA binding channel by smFRET, we placed Cy3 and Cy5 fluorescence labels in the RecA1 domain and the winged-helix (WH) domain located in the C-terminal region of Prp43 from *Chaetomium thermophilum* (ctPrp43) (Figure 2). We generated two maleimide-reactive fluorescence-labeling sites by introducing cysteine residues at positions K170 and E602. To achieve selective labeling, we had to consider the eight native cysteine residues within ctPrp43. C148, C214 and C377 are buried inside the protein, inaccessible to the maleimide coupling group and remained in their native state. C303, C323, C441, C508, and C543 are exposed on the protein surface and were replaced by site directed mutagenesis (C303T, C323V, C441A, C508A and C543S). Furthermore, we attached a non-cleavable histidine-tag (His_6) to the C-terminus of the protein, which allows immobilization of Prp43 on glass coverslips. The resulting Prp43 variant ($Prp43_{Cys}$) was labeled with a mixture of Cy3- and Cy5-maleimide, yielding dual-labeled $Prp43_{Cys}$ with labeling efficiencies of 81% Cy3 and 98% Cy5, respectively as determined by photometrical analysis. In a previous study we have shown that the protein is stable during the labeling process and in smFRET experiments (18). The chosen label positions undergo a large distance change during opening of the channel (Figure 2). Comparison of crystal structures of ctPrp43 in complex with ADP-BeF_3^- in the presence (channel closed) and absence (channel open) of ssRNA revealed that the distance between the C_α atoms of K170 in RecA1 and E602 in WH increases from 3.7 nm in the closed channel structure to 5.4 nm in the open channel structure (closed: PDB: 5lta; open: PDB:5ltk; (16)). The Cy3/Cy5 FRET dye pair has a Förster radius (R_0) of approximately 5.4 nm (36) and is therefore highly suitable to analyze this range of movement.

ATPase activity, RNA binding and RNA unwinding by $Prp43_{cys}$

To ensure that the functionality of $Prp43_{Cys}$ is comparable to Prp43(wt), we measured the rates of ATP turnover by $Prp43_{Cys}$ and Cy3/Cy5-labeled $Prp43_{Cys}$ and addressed how far ATP hydrolysis can be stimulated by the presence of the G-patch factor Pfa1(gp) and the RNA substrate (Figure 3A). The low basic ATPase activity of $Prp43_{Cys}$ increases about 50-fold in the presence of Pfa1(gp) and about 1000-fold in the presence of Pfa1(gp) and ssRNA, which is similar to Prp43(wt) and indicates that the catalytic activity is neither impaired by the mutations nor by the fluorescence tags (Figure 3A). The binding affinity of $Prp43_{Cys}$ for ssRNA was in the μM range without Pfa1(gp) and increased strongly by addition of Pfa1(gp) (K_D = 25 μM and K_D = 0.02 μM, respectively, Figure 3B). Binding of ADP generally reduces the affinity of $Prp43_{Cys}$ for RNA, leading to an extremely high dissociation constant (K_D > 100μM) without the G-patch and a moderate dissociation constant of the $Prp43_{Cys}$-Pfa1(gp) complex (K_D = 0.4 μM). K_D values of $Prp43_{Cys}$ overall agree with values of Prp43(wt) (Figure 3B) and with previous measurements on ctPrp43 and the human homologue DHX15 with its G-patch factor NKRF (17,26). Hence, the general RNA binding properties of $Prp43_{Cys}$ are not substantially changed by the mutations, albeit they seem to some extent decrease the already weak RNA affinity in absence of Pfa1(gp) (Figure 3B). Finally, we monitored the unwinding of a dsRNA substrate with a 3′ ss overhang using the fluorescence-based assay described above. In absence of Pfa1(gp), both Prp43(wt) and $Prp43_{Cys}$ unwind the substrate extremely slow (k_{obs} = 0.03 min^{-1}and k_{obs} = 0.04 min^{-1} respectively; Figure 3C), while the addition of Pfa1(gp) leads to comparably faster unwinding (k_{obs} = 4.6 min^{-1} and k_{obs} = 3.9 min^{-1}). This indicates a strong stimulation of Prp43 helicase activity by Pfa1(gp) and is in line with previous measurements of ctPrp43 activity (16,35). In summary, the central determinants of Prp43 function as assayed here, i.e. the ability to bind and hydrolyze ATP, to bind and unwind RNA and the stimulation of these functions by the G-patch factor Pfa1(gp) are very similar in $Prp43_{Cys}$ and the wild-type counterpart. This allows us to interpret the smFRET data obtained in this study in the context of the functional wt protein.

The Prp43 RNA binding channel shows a dynamic equilibrium between open and closed conformations

To monitor smFRET signals reporting on the structural dynamics of the RNA binding channel in Prp43 by Total Internal Reflection of Fluorescence (TIRF) microscopy, we immobilized Cy3/Cy5-labeled $Prp43_{Cys}$ on neutravidin-functionalized glass cover slips (31). To this end, we attached a biotin-conjugated antibody directed against the C-terminal His_6-tag of $Prp43_{Cys}$ to the neutravidin-coated

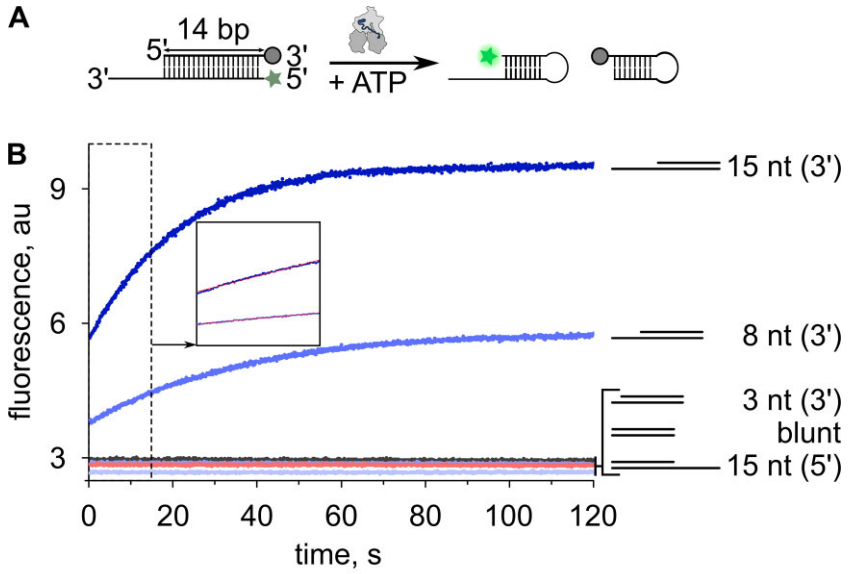

3'-overhang	k_{obs} ,min^{-1}	R^2, linear fit
15 nt	4.6±0.2	0.991±0.001
8 nt	1.2±0.2	0.982±0.004

Figure 1. Prp43 requires a sufficiently long 3′-overhang to unwind RNA duplexes. (**A**) Experiment scheme: Duplex RNA constructs are labeled by ATTO488 (green star) and Eclipse quencher (grey circle). Unwinding is initiated by addition of ATP. The separation of duplex strands becomes apparent by dequenching of the ATTO488 fluorophore (bright green star). Single strands fold into stem-loops to prevent reannealing. (**B**) Time course of fluorescence changes during unwinding of duplex constructs by Prp43-Pfa1(gp) complex. Blue traces: Duplex constructs with 3′ overhangs (15, 8 and 3nt) or blunt ends. Red trace: Duplex construct with 15 nt 5′-overhang. Black trace: Duplex construct with 15 nt 3′-overhang was mixed with Prp43-Pfa1(gp) complex without addition of ATP. Inset shows linear fit of the first 15 s of the time courses. This initial slope was used to calculate the initial unwinding velocity (k_{obs} ± sd, obtained in $n = 3$ independent measurements) shown in the table.

surface (Figure 4). In a previous study we have shown that the His_6-tag does not interfere with Prp43 function (18). The fluorescence labels generate a high FRET signal in the closed state and a low FRET signal in the open state. To elucidate under which conditions channel opening occurs and how this movement is regulated, we monitored E_{FRET} of the labeled molecules in presence and absence of Pfa1(gp), ssRNA and different nucleotides.

First, we analyzed the conformation of the RNA binding channel in Prp43 in absence of ligands. We observed two populations of smFRET signals with $E_{FRET} = 0.89 \pm 0.02$ and $E_{FRET} = 0.57 \pm 0.02$ (Figure 5A, Supplementary Table S1, Supplementary Figure S1A and B), indicating the presence of two structurally distinct states. Based on these values we estimated the Cy3–Cy5 distance in the two states using the Förster equation (37). The high FRET state corresponds to a distance of 3.8 nm, comparable to the distance between the C_α atoms of the labeled residues in the closed state structure of ctPrp43—ADP ($D_{C\alpha}$ = 3.2 nm, PDB: 5d0u (16), Supplementary Table S2). The low FRET state corresponds to a distance of 5.2 nm, which is in good agreement with the open state structures of ctPrp43—ADPBeF$_3^-$ ($D_{C\alpha}$ = 5.1 nm, PDB: 5ltj, and $D_{C\alpha}$ = 5.4 nm, PDB: 5ltk (16), Supplementary Table S2). Although the majority of the helicase molecules (87%, Supplementary Table S1) show a closed binding channel, in a small but significant fraction of molecules the channel is open. So far, the open conformation of the RNA binding channel was only observed in the structures of ctPrp43 bound to the ATP hydrolysis transition state analogue ADP-BeF$_3^-$ and of the DEAH-box helicase Dhr1 in the apo state (16,25). The fact that we can monitor the open conformation by smFRET shows that this state occurs indeed in physiological solution. A small fraction of smFRET traces (5%) shows transitions between open and closed states (Supplementary Figure S1C and D), suggesting the presence of an equilibrium with slow exchange between the populations. While the closed channel conformation seems to be favored under these conditions, the open state is also transiently occupied. This is in line with the existence of apo state DEAH-box helicase structures with both closed and open RNA binding channel (17,25). The dynamics of the equilibrium might be influenced by the binding partners of the helicase, i.e. G-patch, nucleotide or ssRNA, providing a basis for regulation. To test if the interaction with a G-patch partner alters the observed equilibrium, we next monitored E_{FRET} of the Prp43–Pfa1(gp) complex. The fraction of the helicase molecules in the open state increased notably from 15% to 24% compared to the apo protein, and more molecules (9%) showed transitions from the closed towards the open state (Figure 5B, Supplementary Figure S2A, Supplementary Table S1). For some molecules we

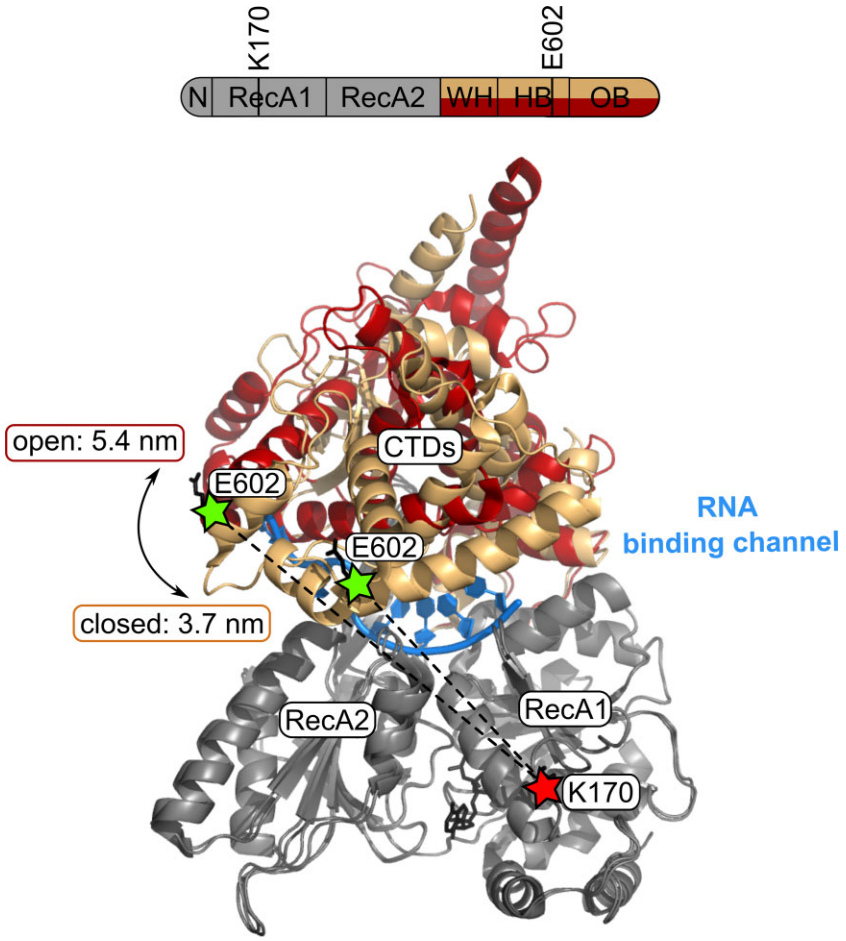

Figure 2. Open to closed transition of the RNA binding channel in Prp43. Domain organization and structure of ctPrp43 (residues 61–764) in complex with ADP-BeF_3^- in presence and absence of U_7-RNA (PDB: 5lta, 5ltk). The truncated N-terminal domain (residues 61–96) and the RecA domains are shown in grey, (RecA1: residues 97–273; RecA2: residues 274–458). The C-terminal domains (winged-helix (WH): residues 459–526, helix-bundle (HB): residues 527–640, and oligosaccharide-binding-fold (OB): residues 641–764) are shown beige for the RNA-bound (closed) structure and in red for the RNA-free (open) structure. Cy3- and Cy5-label positions at K170 and E602 are indicated as red and green stars. The distances between the label positions are indicated as dashed lines.

observed more than one transition, confirming that the channel can reversibly toggle between open and closed conformations, exhibiting an equilibrium (Supplementary Figure S1E and F). Interestingly, when we added ssRNA to the complex, we observed the reverse trend and the fraction of Prp43 molecules with an open channel decreased to 8% while less molecules (3%) showed transitions (Figure 5C, Supplementary Table S1). Additionally, the E_{FRET} values of the closed state show a small shift from $E_{FRET} = 0.89$ observed in the previous conditions to $E_{FRET} = 0.85$ (Figure 5D, Supplementary Table S1). This value corresponds to an increase of the Cy3–Cy5 distance by 0.2–4.0 nm (Supplementary Table S2) suggesting that the fluorophores move further apart when the binding channel closes around the RNA. Indeed, this interpretation is supported by comparison of the Prp43—ADP and Prp43—ADPBeF$_3^-$—ssRNA structures, where the distance between the C_α atoms of the labeled residues increases by 0.4 nm (Supplementary Table S2) (16,29). In the absence of Pfa1(gp) the distribution of FRET values of the Prp43-RNA complex is similar to the apo state (Supplementary Figure S3, Supplementary Table S1). Given the low affinity of $Prp43_{Cys}$ for ssRNA in absence of Pfa1(gp) (Figure 3B) this expectably indicates that only a minor amount of the present RNA is stably bound under the observed conditions.

Together, our data support the idea that the RNA binding channel in Prp43 can alternate between open and closed conformations. The co-factor Pfa1(gp) modulates the equilibrium of these structural states promoting the channel opening. Based on our distance estimations ($E_{FRET} = 0.57$; $D_{D-A} \approx 5.2$ nm, Supplementary Tables S1, S2), the channel opens wide enough for ssRNA to enter in one step. This argues against a mechanism where RNA binding occurs by threading through the opening of a closed channel.

The interplay of ATP and Pfa1(gp) leads to efficient RNA loading and stable binding

Next, we addressed how nucleotide binding influences the conformation of the RNA binding channel (Figure 6). In presence of ATP, E_{FRET} values and the population distribution indicate a clear shift of the equilibrium towards the open state (Figure 6A, Supplementary Table S1). Here,

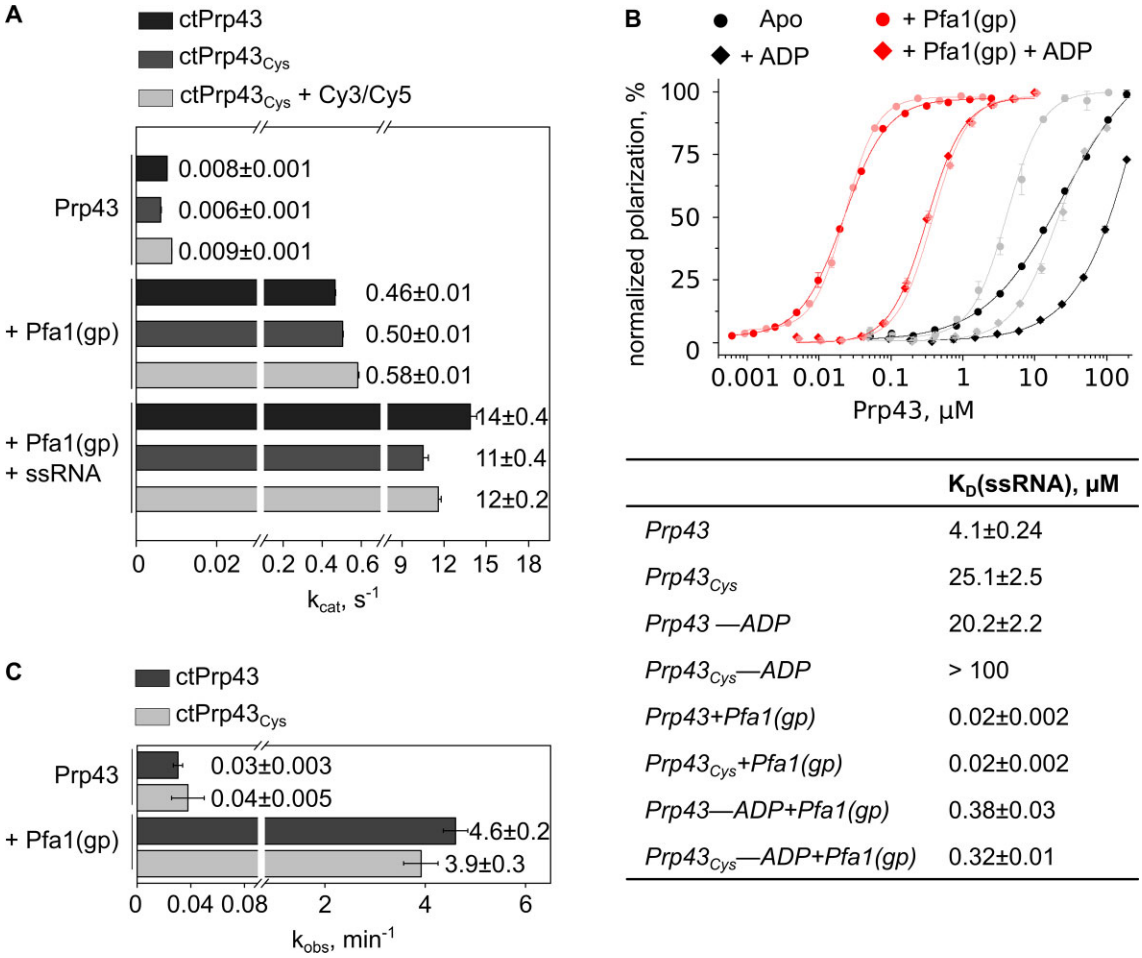

	K_D(ssRNA), μM
Prp43	4.1±0.24
Prp43$_{Cys}$	25.1±2.5
Prp43 —ADP	20.2±2.2
Prp43$_{Cys}$—ADP	> 100
Prp43+Pfa1(gp)	0.02±0.002
Prp43$_{Cys}$+Pfa1(gp)	0.02±0.002
Prp43—ADP+Pfa1(gp)	0.38±0.03
Prp43$_{Cys}$—ADP+Pfa1(gp)	0.32±0.01

Figure 3. Prp43$_{Cys}$ shows wt-like ATPase activity, RNA binding and unwinding. (**A**) Steady-state ATP hydrolysis rates of Prp43, Prp43$_{Cys}$, and Cy3/Cy5-labeled Prp43$_{Cys}$ at 2 mM ATP, determined using a coupled enzymatic assay. Pfa1(gp) and poly-U ssRNA were added at saturating concentrations. k_{cat} ± sd were obtained in $n = 3$ independent measurements. (**B**) Prp43$_{Cys}$ (dark shade) and Prp43 wt (light shade) binding affinity to poly-U ssRNA determined by fluorescence polarization spectroscopy in the absence (black) or presence (red) of Pfa1(gp) in the nt-free (circles) or ADP-bound (squares) state. Mean values derived from $n = 3$ independent measurements are shown; error bars correspond to the sd. The measured polarization was normalized by the maximum value. Affinity constants (K_D(ssRNA)±sd) are indicated in the table. (**C**) Unwinding of a 15 nt RNA duplex with 15 nt 3′-ss overhang by Prp43 and Prp43$_{Cys}$ monitored in a fluorescence-based assay in absence and presence of Pfa1(gp). k_{obs} ± sd were obtained in $n = 3$ independent measurements.

32% of the population adopted the open conformation and an increased fraction of molecules showed transitions between conformations, most of them corresponding to opening of the channel (9%, Supplementary Table S1, Supplementary Figure S2B). In presence of ADP or the non-hydrolysable ATP analog AMPPNP, the population distributions of open and closed conformations are similar to the ATP state, although the open conformations are slightly less populated (21% and 24%, respectively; Supplementary Figure S4A and B, Supplementary Table S1). This indicates that the presence of a nucleotide is sufficient to push the equilibrium towards channel opening, while hydrolysis is not required. Addition of RNA to the Prp43–ATP complex slightly shifted the equilibrium back towards the closed state (19% open), while the fraction of molecules showing transitions remained almost unchanged (Supplementary Figure S5A, Supplementary Figure S2C, Supplementary Table S1). The shift in the population distribution suggests that a fraction of the RNA is bound by the helicase, presumably because ATP-induced channel opening improved the efficiency of RNA loading. Interestingly, in both ATP containing conditions, a very small fraction of the helicase population shows a state with a very low E_{FRET} around 0.25 (Supplementary Figure S2B and C). Visual inspection of traces showed that this state is only transiently sampled, which indicates that in presence of ATP the binding channel can open even further than in the previously studied conditions or as seen in the crystal structures (PDB: 5ltj and 5ltk (16)), leading to estimated Cy3–Cy5 distances of up to 6.5 nm. The addition of Pfa1(gp) to the Prp43—ATP complex did not significantly change the FRET efficiencies and the distribution of states (Figure 6B, Supplementary Table S1). However, less of the extreme wide opening events were observed than in the absence of Pfa1(gp) (Supplementary Figure S2D). It is therefore conceivable that the G-patch restricts the opening range of the channel. This could increase the productivity of the RNA binding as the distance between the RNA backbone interacting with the RecA domains and the HB domain forming the upper side of the binding channel would be restrained.

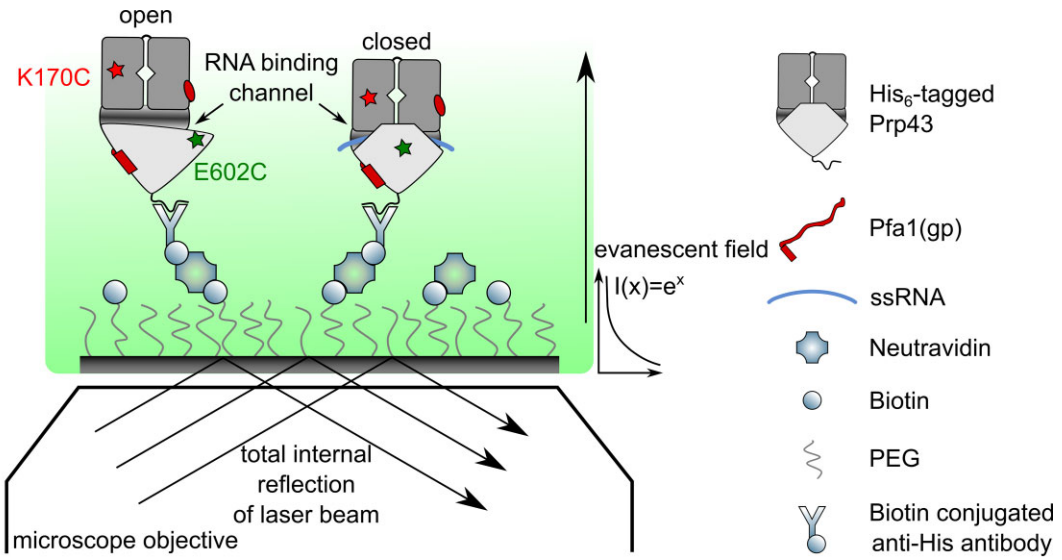

Figure 4. Experimental setup to monitor structural changes of the RNA binding channel in Prp43. TIRF microscopy experiment scheme monitoring conformational changes of the RNA binding channel in Prp43 by smFRET. Labeled $Prp43_{Cys}$ is immobilized on PEG/PEG-Biotin functionalized glass cover slips, using neutravidin to connect a biotinylated antibody directed against the C-terminal His_6-tag of Prp43. A high FRET signal reports on a low Cy3–Cy5 distance corresponding to a closed conformation of the binding channel. Opening of the channel increases the fluorophore distance, leading to a decrease of the FRET signal.

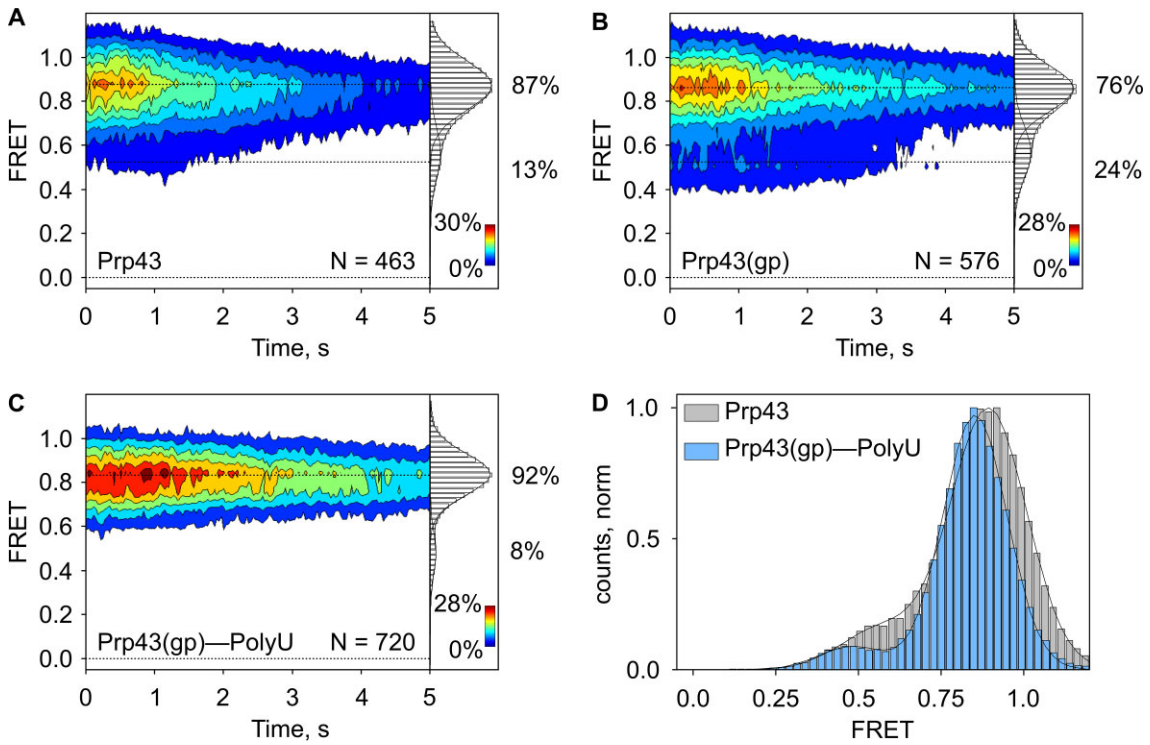

Figure 5. Pfa1(gp) and RNA modulate the conformation of the RNA binding channel. (A–C) Contour plots and 2D histograms showing the distribution of FRET values (mean ± sd) of (**A**) Prp43 in the apo state (0.89 ± 0.02 and 0.57 ± 0.02 with population distributions of 0.87 ± 0.01 and 0.13 ± 0.01 respectively). (**B**) Prp43–Pfa1(gp) complex (0.89 ± 0.01 and 0.57 ± 0.02 with population distributions of 0.76 ± 0.04 and 0.24 ± 0.04 respectively), and (**C**) Prp43–PolyU–Pfa1(gp) complex (0.85 ± 0.01 and 0.48 ± 0.02 with population distributions of 0.92 ± 0.03 and 0.08 ± 0.03 respectively). Normalization was performed here and in all further FRET distributions by the number of FRET counts. *N* here and all further plots indicates the number of individual traces. Data are from $n = 3$ independent experiments. (**D**) Overlay of 2D histograms showing the distribution of FRET values (mean ± sd) of Prp43 in absence and presence of Pfa1(gp) and ssRNA. The center of the closed state shifts from $E_{FRET} = 0.89 \pm 01$ to $E_{FRET} = 0.85 \pm 01$.

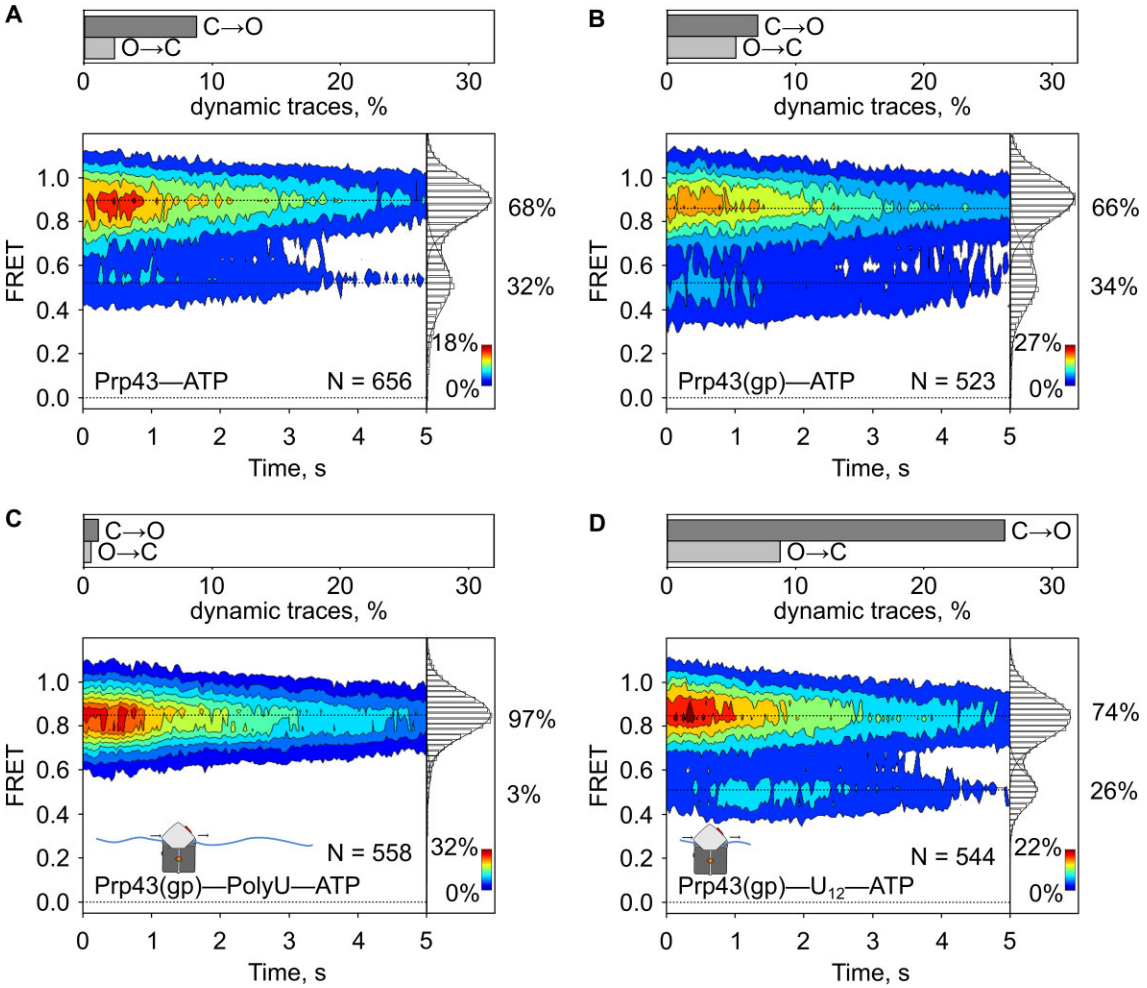

Figure 6. Influence of ATP on the conformation of the RNA binding channel. (A–D) Transition frequency (above) and contour plots and 2D histograms (below) showing the distribution of FRET values (mean ± sd) of (**A**) Prp43–ATP (0.90 ± 0.01 and 0.52 ± 0.01 with population distributions of 0.68 ± 0.01 and 0.32 ± 0.01 respectively). (**B**) Prp43–ATP–Pfa1(gp) (0.90 ± 0.01 and 0.54 ± 0.04 with population distributions of 0.66 ± 0.02 and 0.34 ± 0.02 respectively). (**C**) Prp43–ATP–PolyU–Pfa1(gp) (0.85 ± 0.01 and 0.57 ± 0.03 with population distributions of 0.97 ± 0.01 and 0.03 ± 0.01 respectively) and (**D**) Prp43–ATP–U12–Pfa1(gp) (0.86 ± 0.02 and 0.52 ± 0.01 with population distributions of 0.74 ± 0.04 and 0.26 ± 0.04 respectively). The transition frequencies were determined by dividing the total number of transitions between closed and open conformation observed in one condition by the total number of traces (N) of that condition.

In fact, when we added PolyU ssRNA to the Prp43–ATP–Pfa1(gp) complex, nearly the entire Prp43 population (97%) shows the closed channel conformation previously observed upon stable RNA binding by the Prp43–Pfa1(gp) complex ($E_{FRET} = 0.85$, Figure 5C), while almost no transitions occur (Figure 6C, Supplementary Table S1). While Prp43 performs rapid ATP turnover under these conditions (Figure 3A), the interplay of Pfa1(gp) and RNA seems to lock the channel in a closed conformation, keeping it stably bound around the RNA substrate during translocation. Interestingly, when substituting the long PolyU RNA used in the previous experiment with shorter U_{12} RNA the population distribution is clearly shifted towards channel opening and the fraction of molecules showing transitions is increased to 32% (Figure 6D, Supplementary Table S1). While molecules that showed dynamic behavior populated both states almost equally, the molecules that retained their channel conformation during the course of the experiment predominantly exhibited the closed state (Supplementary Figure S5B and C). Most transitions corresponded to opening of the channel (Supplementary Figure S5D). Taken together, these observations indicate that after staying closed during complete translocation across one RNA strand and release of that strand, the binding channel opens again to facilitate the rebinding of another RNA molecule. Traces showing transitions following this suggested sequence of events further support this interpretation (Supplementary Figure S5E). To confirm that the increased dynamic was caused by RNA release and rebinding due to translocation we also studied the effect of extremely short RNA strands. We fragmented U_{12} RNA by sonication to obtain strands that were too short for translocation as they did not fill the complete RNA binding channel. When adding these fragments to the Prp43–ATP–Pfa1(gp) complex, we observed almost exclusively the closed state (92%), while only 3% of the molecules showed transitions (Supplementary Figure S5F, Supplementary Table S1). This indicates that the short strands are stably bound by Prp43, causing a

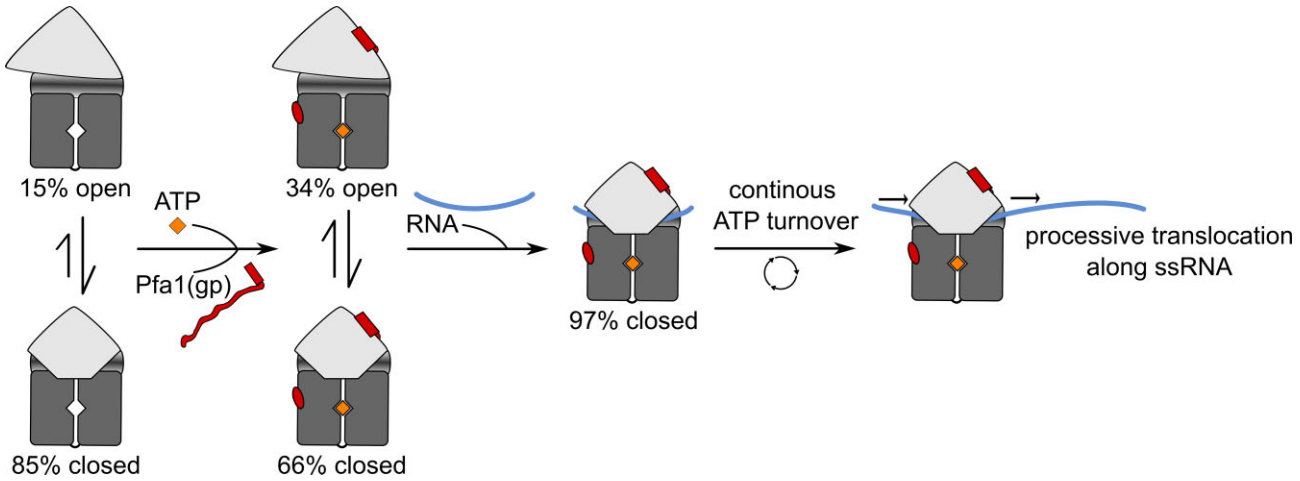

Figure 7. Model of RNA loading by Prp43. In this mechanistic scheme of RNA loading by Prp43, Pfa1(gp) is depicted in red, the RecA and C-terminal domains of Prp43 are colored in shades of grey and the RNA is depicted in blue. The model describes how the interaction with Pfa1(gp) and ATP shifts the RNA binding channel towards an open conformation, increasing the efficiency of RNA loading. In the RNA-bound state, the channel remains closed which allows for processive translocation without losing contact to the ssRNA during continuous ATP turnover. The numbers indicate the distributions of molecules observed in the smFRET experiments reported in Figures 5 and 6.

predominantly closed channel conformation, while no translocation occurs.

In summary, our data show that in the absence of the RNA substrate ATP binding strongly shifts the dynamic equilibrium of channel conformations towards the open state, resulting in an increased part of the population being primed for RNA loading. While the G-patch slightly reinforces this effect, it likely also restricts the opening range of the channel to facilitate efficient RNA loading. Upon binding of the RNA substrate, the G-patch supports the closed channel conformation to allow stable binding which is an essential prerequisite for processive motion. Following release of the RNA substrate after complete translocation, the equilibrium is again shifted towards channel opening, facilitating efficient loading of the next RNA strand.

DISCUSSION

RNA loading mechanism of Prp43

In the present study we investigated in more detail the loading and binding properties of Prp43 to RNA. Our data show that in the absence of ligands and co-factors the RNA binding channel in Prp43 can exist in two different conformations, which we denominate the open and closed states. Apo-Prp43 alternates slowly between the two states, but shows a strong preference for the closed state (Figure 7). Binding of the co-factor Pfa1(gp) slightly shifts the dynamic equilibrium of channel conformations towards the open state. Binding of ATP to the Prp43–Pfa1(gp) complex further enhances channel opening. The subsequent accommodation of ssRNA promotes the closure of the channel, and the open state is nearly absent indicative of the productive loading of the helicase onto ssRNA. A direct comparison with our previous study characterizing the motility of the RecA domains of Prp43 (18) reveals that the dynamic of the RNA binding channel observed here is completely independent from the internal movements of the helicase core. While the RecA domains continuously cycle between open and closed conformations during ATP turnover, facilitating translocation (17,18), the binding channel stays closed around the RNA substrate, ensuring stable binding of Prp43. After reaching the end of an RNA strand, Prp43 returns to the dynamic equilibrium between open and closed channel conformations until a new substrate is bound. In the absence of the G-patch, the closure of the channel around RNA is rarely observed and Prp43 dissociates rapidly (18). This prevents futile interactions with RNA when unwinding is not required. Hence, the main function of the G-patch in the absence of RNA relates to the opening of the channel prior to RNA binding. However, in the presence of RNA Pfa1(gp) stabilizes the closed state as interactions between the RNA and residues of the tunnel are not sufficient to maintain the closed state during turnover. Closure of the channel during continuous turnover enables Prp43 translocation along ssRNA without detachment.

Role of the G-patch

Besides shifting the conformation of Prp43 towards channel opening, the G-patch likely is responsible for the channel to stay closed around RNA, even during continuous ATP turnover. Prp2 is a further DEAH-box family member known to interact with a G-patch partner. Despite a similar binding mode of the G-patch motif, the interaction with the helicase Prp2 shows striking differences (26,38). In contrast to the G-patch partners of Prp43, the G-patch protein Spp2 does not stimulate the ATPase activity of Prp2 on its own, instead it requires the presence of ssRNA (39). A comparison between cryo-EM structures of Prp2 in presence and absence of Spp2 showed no differences in the overall conformation of the helicase (40). However, due to a lack of real-time data an impact of Spp2 on the domain motility of Prp2 cannot be excluded. As Prp2 has higher affinity for ssRNA than Prp43 that is not influenced by the presence of Spp2 (39), the G-patch interaction likely is not needed

for Prp2 to maintain a stable grip on the RNA. Presumably, tethering Prp2 close to its target site in the spliceosome is more relevant than directly altering its conformational dynamic. DEAH-box helicases that have no G-patch partner either need to maintain the stable RNA interaction during translocation on their own or might be supported by other cofactors. For example, UTP14A is the co-factor of Dhr1/DHX37 and enhances ATP hydrolysis as well as RNA binding and unwinding and might therefore play a similar role as Pfa1 in RNA loading (41,42). However, the affinity of Dhr1/DHX37 to RNA in the absence of cofactors is considerably higher compared to Prp43, suggesting that it might stay bound on the RNA during ATP turnover without assistance of a co-factor (41).

Comparison to other SF2 helicases

Crystal structures of other DEAH-box helicases support our finding that the RNA binding channel can alternate between open and closed conformations. A closed channel conformation was observed for the spliceosomal helicase Prp22 in the apo state (17), while apo-Dhr1 (DHX37 in humans), a DEAH-box helicase acting in ribosome assembly, showed an open channel (25). As the RNA interaction mode is conserved in the DEAH-box family of helicases (16,17,41) a common mechanism of RNA loading is highly probable. Loading of the RNA into an open channel is advantageous compared to threading of a single strand through the entrance of the closed channel and thus allows DEAH-box helicases to access their cellular binding sites within large RNP structures efficiently. In contrast to DEAD-box helicases, most of which bind RNA solely with their RecA domains, other processive superfamily 2 helicases bind ssRNA in a similar manner to DEAH-box helicases, i.e. in a cleft formed between the helicase core and their respective C-terminal domains. Examples are the Ski2-like helicases Hel308 and Mtr4, involved in DNA repair and nuclear RNA processing, or the NS3 helicase of hepatitis C virus (28,43–47). Comparison between NS3 helicases from different hepatitis C virus strains showed that slight changes in the electrostatic properties of the RNA binding channel can have a huge impact on the efficiency of RNA binding and unwinding, indicating that helicase activity is regulated by variations in the RNA binding channel (48).

Overall, the initial RNA loading step has a huge impact on the unwinding properties of a helicase and provides diverse means of regulation, thereby fine-tuning its cellular function. Here, we provide a mechanistic model of RNA loading by Prp43 which can facilitate the understanding of this process for related helicases involved in many critical steps of RNA metabolism.

DATA AVAILABILITY

The data underlying this article are available in the article and in its online supplementary material.

SUPPLEMENTARY DATA

Supplementary Data are available at NAR Online.

ACKNOWLEDGEMENTS

We thank Prof. M. Rodnina for access to the TIRF microscopy facility in her department. We thank Dr A. Dickmanns for critically reading of the manuscript.

FUNDING

German Research Council (Deutsche Forschungsgemeinschaft) with project grants [SFB860, project A2 to R.F., SFB860, project A15 to S.A.]. Funding for open access charge: Deutsche Forschungsgemeinschaft [SFB860].
Conflict of interest statement. None declared.

REFERENCES

1. Bohnsack,K.E., Kanwal,N. and Bohnsack,M.T. (2022) Prp43/DHX15 exemplify RNA helicase multifunctionality in the gene expression network. *Nucleic Acids Res.*, **50**, 9012–9022.
2. Pyle,A.M. (2008) Translocation and unwinding mechanisms of RNA and DNA helicases. *Annu. Rev. Biophys.*, **37**, 317–336.
3. De Bortoli,F., Espinosa,S. and Zhao,R. (2021) DEAH-Box RNA helicases in pre-mRNA splicing. *Trends Biochem. Sci.*, **46**, 225–238.
4. Robert-Paganin,J., Halladjian,M., Blaud,M., Lebaron,S., Delbos,L., Chardon,F., Capeyrou,R., Humbert,O., Henry,Y., Henras,A.K. *et al.* (2017) Functional link between DEAH/RHA helicase Prp43 activation and ATP base binding. *Nucleic Acids Res.*, **45**, 1539–1552.
5. Chen,Y.-L.L., Capeyrou,R., Humbert,O., Mouffok,S., Kadri,Y.A., Lebaron,S., Henras,A.K. and Henry,Y. (2014) The telomerase inhibitor Gno1p/PINX1 activates the helicase Prp43p during ribosome biogenesis. *Nucleic Acids Res.*, **42**, 7330–7345.
6. Bohnsack,M.T., Martin,R., Granneman,S., Ruprecht,M., Schleiff,E. and Tollervey,D. (2009) Prp43 bound at different sites on the pre-rRNA performs distinct functions in ribosome synthesis. *Mol. Cell*, **36**, 583–592.
7. Pertschy,B., Schneider,C., Gnädig,M., Schäfer,T., Tollervey,D. and Hurt,E. (2009) RNA helicase Prp43 and its co-factor Pfa1 promote 20 to 18 S rRNA processing catalyzed by the endonuclease Nob1. *J. Biol. Chem.*, **284**, 35079–35091.
8. Lebaron,S., Papin,C., Capeyrou,R., Chen,Y.-L., Froment,C., Monsarrat,B., Caizergues-Ferrer,M., Grigoriev,M. and Henry,Y. (2009) The ATPase and helicase activities of Prp43p are stimulated by the G-patch protein Pfa1p during yeast ribosome biogenesis. *EMBO J.*, **28**, 3808–3819.
9. Wan,R., Yan,C., Bai,R., Lei,J. and Shi,Y. (2017) Structure of an intron lariat spliceosome from saccharomyces cerevisiae. *Cell*, **171**, 120–132.
10. Tanaka,N., Aronova,A. and Schwer,B. (2007) Ntr1 activates the Prp43 helicase to trigger release of lariat-intron from the spliceosome. *Genes Dev.*, **21**, 2312–2325.
11. Fourmann,J.B., Dybkov,O., Agafonov,D.E., Tauchert,M.J., Urlaub,H., Ficner,R., Fabrizio,P. and Lührmann,R. (2016) The target of the DEAH-box NTP triphosphatase Prp43 in saccharomyces cerevisiae spliceosomes is the U2 snRNP-intron interaction. *Elife*, **5**, e15564.
12. Mayas,R.M., Maita,H., Semlow,D.R. and Staley,J.P. (2010) Spliceosome discards intermediates via the DEAH box ATPase Prp43p. *Proc. Natl. Acad. Sci. U.S.A.*, **107**, 10020–10025.
13. Fourmann,J.-B.B., Tauchert,M.J., Ficner,R., Fabrizio,P. and Lührmann,R. (2017) Regulation of Prp43-mediated disassembly of spliceosomes by its cofactors Ntr1 and Ntr2. *Nucleic Acids Res.*, **45**, 4068–4080.
14. Arenas,J.E. and Abelson,J.N. (1997) Prp43: an RNA helicase-like factor involved in spliceosome disassembly. *Proc. Natl. Acad. Sci. U.S.A.*, **94**, 11798–11802.
15. He,Y., Staley,J.P., Andersen,G.R. and Nielsen,K.H. (2017) Structure of the DEAH/RHA ATPase Prp43p bound to RNA implicates a pair of hairpins and motif Va in translocation along RNA. *RNA*, **23**, 1110–1124.
16. Tauchert,M.J., Fourmann,J.B., Lührmann,R. and Ficner,R. (2017) Structural insights into the mechanism of the DEAH-box RNA helicase Prp43. *Elife*, **6**, e21510.

17. Hamann,F., Enders,M. and Ficner,R. (2019) Structural basis for RNA translocation by DEAH-box ATPases. *Nucleic Acids Res.*, **47**, 4349–4362.
18. Enders,M., Ficner,R. and Adio,S. (2022) Regulation of the DEAH/RHA helicase Prp43 by the G-patch factor Pfa1. *Proc. Natl. Acad. Sci. U.S.A.*, **119**, e2203567119.
19. Christian,H., Hofele,R.V., Urlaub,H. and Ficner,R. (2014) Insights into the activation of the helicase Prp43 by biochemical studies and structural mass spectrometry. *Nucleic Acids Res.*, **42**, 1162–1179.
20. Tsai,R.-T., Tseng,C.-K., Lee,P.-J., Chen,H.-C., Fu,R.-H., Chang,K., Yeh,F.-L. and Cheng,S.-C. (2007) Dynamic Interactions of Ntr1-Ntr2 with Prp43 and with U5 Govern the Recruitment of Prp43 To Mediate Spliceosome Disassembly. *Mol. Cell. Biol.*, **27**, 8027–8037.
21. Aravind,L. and Koonin,E.V. (1999) G-patch: a new conserved domain in eukaryotic RNA-processing proteins and type D retroviral polyproteins. *Trends Biochem. Sci.*, **24**, 342–344.
22. Tanaka,N. and Schwer,B. (2005) Characterization of the NTPase, RNA-binding, and RNA helicase activities of the DEAH-box splicing factor Prp22. *Biochemistry*, **44**, 9795–9803.
23. Smaldino,P.J., Routh,E.D., Kim,J.H., Giri,B., Creacy,S.D., Hantgan,R.R., Akman,S.A. and Vaughn,J.P. (2015) Mutational dissection of telomeric DNA binding requirements of G4 Resolvase 1 shows that G4-structure and certain 3′-tail sequences are sufficient for tight and complete binding. *PLoS One*, **10**, e0132668.
24. Gilman,B., Tijerina,P. and Russell,R. (2017) Distinct RNA-unwinding mechanisms of DEAD-box and DEAH-box RNA helicase proteins in remodeling structured RNAs and RNPs. *Biochem. Soc. Trans.*, **45**, 1313–1321.
25. Roychowdhury,A., Joret,C., Bourgeois,G., Heurgué-Hamard,V., Lafontaine,D.L.J. and Graille,M. (2019) The DEAH-box RNA helicase Dhr1 contains a remarkable carboxyl terminal domain essential for small ribosomal subunit biogenesis. *Nucleic Acids Res.*, **47**, 7548–7563.
26. Studer,M.K., Ivanovic,L., Weber,M.E., Marti,S. and Jonas,S. (2020) Structural basis for DEAH-helicase activation by G-patch proteins. *Proc. Natl. Acad. Sci. U.S.A.*, **117**, 7159–7170.
27. Heininger,A.U., Hackert,P., Andreou,A.Z., Boon,K.L., Memet,I., Prior,M., Clancy,A., Schmidt,B., Urlaub,H., Schleiff,E. *et al.* (2016) Protein cofactor competition regulates the action of a multifunctional RNA helicase in different pathways. *RNA Biol.*, **13**, 320–330.
28. Appleby,T.C., Anderson,R., Fedorova,O., Pyle,A.M., Wang,R., Liu,X., Brendza,K.M. and Somoza,J.R. (2011) Visualizing ATP-dependent RNA translocation by the NS3 helicase from HCV. *J. Mol. Biol.*, **405**, 1139–1153.
29. Tauchert,M.J., Fourmann,J.B., Christian,H., Lührmann,R. and Ficner,R. (2016) Structural and functional analysis of the RNA helicase Prp43 from the thermophilic eukaryote Chaetomium thermophilum. *Acta Crystallogr. Sect. Struct. Biol. Commun.*, **72**, 112–120.
30. Studier,F.W. (2005) Protein production by auto-induction in high density shaking cultures. *Protein Expr. Purif.*, **41**, 207–234.
31. Adio,S., Senyushkina,T., Peske,F., Fischer,N., Wintermeyer,W. and Rodnina,M.V. (2015) Fluctuations between multiple EF-G-induced chimeric tRNA states during translocation on the ribosome. *Nat. Commun.*, **6**, 7442.
32. Roy,R., Hohng,S. and Ha,T. (2008) A practical guide to single molecule FRET. *Nat. Methods*, **5**, 507–516.
33. Bronson,J.E., Fei,J., Hofman,J.M., Gonzalez,R.L. and Wiggins,C.H. (2009) Learning rates and states from biophysical time series: a Bayesian approach to model selection and single-molecule FRET data. *Biophys. J.*, **97**, 3196–3205.
34. Agarwal,K.C., Miech,R.P. and Parks,R.E. (1978) Guanylate kinases from human erythrocytes, hog brain, and rat liver. *Methods Enzymol.*, **51**, 483–490.
35. Hamann,F., Zimmerningkat,L.C., Becker,R.A., Garbers,T.B., Neumann,P., Hub,J.S. and Ficner,R. (2021) The structure of Prp2 bound to RNA and ADP-BeF3-reveals structural features important for RNA unwinding by DEAH-box ATPases. *Acta Crystallogr. Sect. D Struct. Biol.*, **77**, 496–509.
36. Son,H., Mo,W., Park,J., Lee,J.W. and Lee,S. (2020) Single-molecule FRET detection of sub-nanometer distance changes in the range below a 3-nanometer scale. *Biosensors*, **10**, bios10110168.
37. Förster,T. (1946) Energiewanderung und Fluoreszenz. *Naturwissenschaften*, **33**, 166–175.
38. Hamann,F., Schmitt,A., Favretto,F., Hofele,R., Neumann,P., Xiang,S.Q., Urlaub,H., Zweckstetter,M. and Ficner,R. (2020) Structural analysis of the intrinsically disordered splicing factor Spp2 and its binding to the DEAH-box ATPase Prp2. *Proc. Natl. Acad. Sci. U.S.A.*, **117**, 2948–2956.
39. Warkocki,Z., Schneider,C., Mozaffari-Jovin,S., Schmitzová,J., Höbartner,C., Fabrizio,P. and Lührmann,R. (2015) The G-patch protein Spp2 couples the spliceosome-stimulated ATpase activity of the deah-box protein Prp2 to catalytic activation of the spliceosome. *Genes Dev.*, **29**, 94–107.
40. Bai,R., Wan,R., Yan,C., Jia,Q., Lei,J. and Shi,Y. (2021) Mechanism of spliceosome remodeling by the ATPase/helicase Prp2 and its coactivator Spp2. *Science*, **371**, eabe8863.
41. Boneberg,F.M., Brandmann,T., Kobel,L., Van Den Heuvel,J., Bargsten,K., Bammert,L., Kutay,U. and Jinek,M. (2019) Molecular mechanism of the RNA helicase DHX37 and its activation by UTP14A in ribosome biogenesis. *RNA*, **25**, 685–701.
42. Zhu,J., Liu,X., Anjos,M., Correll,C.C. and Johnson,A.W. (2016) Utp14 recruits and activates the RNA helicase Dhr1 to undock U3 snoRNA from the preribosome. *Mol. Cell. Biol.*, **36**, 965–978.
43. Van Hoof,A., Lennertz,P. and Parker,R. (2000) Yeast exosome mutants accumulate 3-extended polyadenylated forms of U4 small nuclear RNA and small nucleolar RNAs. *Mol. Cell. Biol.*, **20**, 441–452.
44. Guy,C.P. and Bolt,E.L. (2005) Archaeal Hel308 helicase targets replication forks in vivo and in vitro and unwinds lagging strands. *Nucleic Acids Res.*, **33**, 3678–3690.
45. Lam,A.M.I. and Frick,D.N. (2006) Hepatitis C virus subgenomic replicon requires an active NS3 RNA helicase. *J. Virol.*, **80**, 404–411.
46. Büttner,K., Nehring,S. and Hopfner,K.P. (2007) Structural basis for DNA duplex separation by a superfamily-2 helicase. *Nat. Struct. Mol. Biol.*, **14**, 647–652.
47. Weir,J.R., Bonneau,F., Hentschel,J., Conti,E. and Feigon,J. (2010) Structural analysis reveals the characteristic features of Mtr4, a DExH helicase involved in nuclear RNA processing and surveillance. *Proc. Natl Acad. Sci. U.S.A.*, **107**, 12139–12144.
48. Zhou,T., Ren,X., Adams,R.L. and Pyle,A.M. (2018) NS3 from hepatitis C virus strain JFH-1 is an unusually robust helicase that is primed to bind and unwind viral RNA. *J. Virol.*, **92**, e01253-17.